Technical University of Denmark

DTU

Cu(II) mediates kinetically distinct, non-amyloidogenic aggregation of amyloid-peptides

Pedersen, Jeppe T.; Østergaard, Jesper; Rozlosnik, Noemi; Gammelgaard, Bente; Heegaard, Niels H. H.

Link back to DTU Orbit

DTU Library
Technical Information Center of Denmark

Cu(II) Mediates Kinetically Distinct, Non-amyloidogenic Aggregation of Amyloid-β Peptides*[S]

Jeppe T. Pedersen[‡], Jesper Østergaard[‡1], Noemi Rozlosnik[§], Bente Gammelgaard[‡], and Niels H. H. Heegaard[¶2]

From the [‡]Department of Pharmaceutics and Analytical Chemistry, Faculty of Pharmaceutical Sciences, University of Copenhagen, Universitetsparken 2, DK-2100 Copenhagen, Denmark, the [§]Department of Micro- and Nanotechnology, Technical University of Denmark, Ørsted plads, DK-2800 Kongens Lyngby, Denmark, and the [¶]Department of Clinical Biochemistry and Immunology, Statens Serum Institut, Artillerivej 5, DK-2300 Copenhagen, Denmark

Cu(II) ions are implicated in the pathogenesis of Alzheimer disease by influencing the aggregation of the amyloid-β (Aβ) peptide. Elucidating the underlying Cu(II)-induced Aβ aggregation is paramount for understanding the role of Cu(II) in the pathology of Alzheimer disease. The aim of this study was to characterize the qualitative and quantitative influence of Cu(II) on the extracellular aggregation mechanism and aggregate morphology of $A\beta_{1-40}$ using spectroscopic, microelectrophoretic, mass spectrometric, and ultrastructural techniques. We found that the Cu(II):Aβ ratio in solution has a major influence on (i) the aggregation kinetics/mechanism of Aβ, because three different kinetic scenarios were observed depending on the Cu(II):Aβ ratio, (ii) the metal:peptide stoichiometry in the aggregates, which increased to 1.4 at supra-equimolar Cu(II):Aβ ratio; and (iii) the morphology of the aggregates, which shifted from fibrillar to non-fibrillar at increasing Cu(II):Aβ ratios. We observed dynamic morphological changes of the aggregates, and that the formation of spherical aggregates appeared to be a common morphological end point independent on the Cu(II) concentration. Experiments with $A\beta_{1-42}$ were compatible with the conclusions for $A\beta_{1-40}$ even though the low solubility of $A\beta_{1-42}$ precluded examination under the same conditions as for the $A\beta_{1-40}$. Experiments with $A\beta_{1-16}$ and $A\beta_{1-28}$ showed that other parts than the Cu(II)-binding His residues were important for Cu(II)-induced Aβ aggregation. Based on this study we propose three mechanistic models for the Cu(II)-induced aggregation of $A\beta_{1-40}$ depending on the Cu(II):Aβ ratio, and identify key reaction steps that may be feasible targets for preventing Cu(II)-associated aggregation or toxicity in Alzheimer disease.

Extracellular cerebral plaques composed mainly of amyloid β-peptide (Aβ) 1–40 and 1–42 fibrils are a histopathological hallmark of Alzheimer disease (AD)[3] (1, 2). These plaques contain elevated levels of metals, in particular zinc and copper (3).

Also, it has been shown that these metal ions can promote the aggregation of Aβ *in vitro* (4, 5). This implies a key role of the metal ions in the Aβ-mediated pathology of AD (6), although the subject is still under much debate (7, 8), and a role of amyloid-independent pathways in AD neurodegeneration have recently been reviewed (9).

Specifically regarding the role of metal ions in the amyloid-mediated pathology of AD, it is believed that Zn(II) acts as a neuroprotector (10, 11), whereas Cu(II) is considered to mediate neurotoxicity (12–14). The latter effect is thought to occur through early stage soluble Aβ and Aβ-Cu oligomeric intermediates (15–18) that may be involved in the formation of reactive oxygen species (6). It was discovered that Cu(II) may be released postsynaptically at glutamatergic synapses in hippocampus (19, 20), the site for initial Aβ deposition in AD. This provides an explanation for how Cu(II) can interact with Aβ. Seemingly in contrast to the support for the neurotoxic effects of Cu(II), recent evidence indicates a neuroprotective role of intracellular Cu(I) via activation of intracellular neuroprotective cell signaling pathways that increase expression of Aβ-degrading proteinases (21). In all events elucidating the underlying molecular mechanisms of the Aβ-Cu, interactions are vital for understanding the role of Cu(II) in the pathology of AD, and hence in developing new therapeutic strategies for the treatment of AD (7, 22). Despite extensive studies, however, these mechanisms remain largely unsettled and conflicting effects have been reported; in some studies Cu(II) appears to be involved in amyloid oligomerization (4, 23, 24), other studies report that Cu(II) does enhance aggregation but only along non-amyloidogenic pathways (17, 25), or even that Cu(II) inhibits the aggregation of Aβ (26). We recently showed that Cu(II) could induce both oligomerization and non-oligomerization pathways of $A\beta_{1-40}$ on the millisecond-second time scale (27). Distinct oligomerization pathways have also been reported for spontaneous oligomerization of Aβ (28–30). These reports show that multiple Aβ oligomerization pathways can co-exist, which could have major importance in understanding the molecular aspects of AD pathology. An intriguing approach for elucidating the complex role of Cu(II) in the Aβ aggregation mechanism would be the use of complementary kinetic methods as advocated in a recent review (31). In particular, kinetic studies on Cu(II) bound to Aβ have been lacking, and to our knowledge only end point determination of the copper content in the amyloid aggregates has been performed (32, 33). Nevertheless, this information is as important as the out-

---

come of studies on the peptide disappearance or aggregation formation kinetics for elucidating the Aβ-Cu(II) interplay and will form the basis for studies of neuro-cytotoxicity under defined metallopeptide conditions.

In this study we investigated the influence of Cu(II) on aggregation kinetics of Aβ *in vitro* on the minutes-days time scale at physiological conditions using a range of biophysical methods in combination with simulations of the reaction kinetics. With the objective of studying the underlying Cu(II)-induced Aβ aggregation mechanisms, we characterized the disappearance kinetics of soluble species (including Cu(II)) as well as the formation kinetics, morphology, ultrastructure, and stability of the emerging fibrils and aggregates in solutions of $A\beta_{1-40}$, $A\beta_{1-42}$, $A\beta_{1-28}$, and $A\beta_{1-16}$ using a combination of spectroscopic, microelectrophoretic, mass spectrometric, and microscopic techniques. We confirm concentration-dependent effects of Cu(II) on the aggregation kinetics of $A\beta_{1-40}$ and $A\beta_{1-42}$. Most importantly, we show for the first time that three different aggregation scenarios exist depending on the Cu(II):Aβ ratio, and that Cu(II) co-aggregates with Aβ. We directly show the decrease in fibrillar structures concomitant with increases in Cu(II) concentrations indicating a destabilizing effect of Cu(II) on amyloid fibrils. Also, dynamic changes in the aggregate morphology, where small, spherical aggregates appeared to be a common end point were observed. Finally, we show that other factors than the Cu(II)-binding His residues are of importance in the Cu(II)-mediated aggregation of Aβ. Based on the obtained kinetic and morphological data, we propose three mechanistic models for the Cu(II)-induced aggregation of $A\beta_{1-40}$ depending on the metal:peptide ratio, and identify key reaction steps that may be potential targets for preventing Cu(II)-induced aggregation in AD. Also, whereas neurotoxicity studies were outside of the scope of the present study we believe that the results are important for conducting such studies under well defined metal-ion conditions.

EXPERIMENTAL PROCEDURES

Peptide Preparation—Synthetic Aβ peptides based on the human sequences ($A\beta_{1-16}$, $A\beta_{1-28}$, $A\beta_{1-40}$, $A\beta_{1-42}$ >95% purity) were obtained from commercial sources (Bachem and Caslo Laboratory). A marker peptide (PSKD) was purchased from Schafer-N. All peptides were C-terminal carboxylic acids and were purchased as lyophilized trifluoroacetate salts. The sequence of each peptide is shown (Scheme 1).

$A\beta_{1-16}$, $A\beta_{1-28}$, and $A\beta_{1-40}$ were handled identically as described below. $A\beta_{1-16/28/40}$ stock solutions were prepared by dissolving ~1 mg of lyophilized peptide in 1.5 ml of 20 mM HEPES buffer (pH 7.40) containing 100 mM sodium chloride. To minimize the presence of both undissolved peptide and pre-formed aggregates (34), the solution was sonicated for 5 min, centrifuged at $14,000 \times g$ for 25 min at 5 °C, and finally filtered (0.22 μm filter). The peptide concentration was determined by UV absorption spectroscopy using the molar extinction coefficient of tyrosine at 276 nm ($\epsilon = 1,410$ M^{-1} cm^{-1}), and diluted with the 20 mM HEPES buffer to the appropriate concentration (40 μM unless stated otherwise) and immediately analyzed by capillary electrophoresis or frozen and stored at -20 °C in smaller aliquots. Prior to use, peptides were thawed at 5 °C, and

1	10	20	30	40

Human $A\beta_{1-42}$
DAEFRHDSGYEVHHQKLVFFAEDVGSNKGAIIGLMVGGVVIA

Human $A\beta_{1-40}$
DAEFRHDSGYEVHHQKLVFFAEDVGSNKGAIIGLMVGGVV

Human $A\beta_{1-28}$
DAEFRHDSGYEVHHQKLVFFAEDVGSNK

Human $A\beta_{1-16}$
DAEFRHDSGYEVHHQK

SCHEME 1.

afterward kept on ice. The peptide solutions were centrifuged at $14,000 \times g$ for 25 min (5) at 5 °C immediately after thawing to remove aggregates formed during thawing. Then, 2/3 of the upper supernatant was removed and mixed with an equal volume of 20 mM HEPES buffer without or with increasing concentrations of Cu(II). The concentration of Aβ was confirmed by reference to a standard curve using capillary electrophoresis (CE). Differences with respect to kinetics or initial peptide concentration between samples that were used immediately upon preparation and samples that had been frozen were not observed at any point. The final concentration of Cu(II) in the samples ranged between 0 and 200 μM. The 10 mM Cu(II) stock solution was prepared from CuCl₂. To prevent formation of Cu(OH)₂ 4 molar eq of glycine were added to the stock solutions (35).

$A\beta_{1-42}$ solutions were prepared by dissolving the lyophilized peptide in high purity water and adjusting the pH to 10.5 with NaOH. The samples were sonicated in ice water for 5 min and centrifuged at $14,000 \times g$ for 25 min at 5 °C. The supernatant was frozen in smaller aliquots and stored at -20 °C until use. Due to the much lower solubility of $A\beta_{1-42}$ at neutral pH, all the $A\beta_{1-42}$ experiments were performed at pH 10.5. Cu(II) solutions used for experiments with $A\beta_{1-42}$ was prepared from CuCl₂ dissolved in high purity water.

Capillary Electrophoresis—CE experiments were performed using a P/ACE MDQ CE instrument (Beckman Coulter). Electrophoresis buffer was 20 mM HEPES (pH 7.4) containing 100 mM sodium chloride. UV detection was performed at $\lambda = 200$ nm. Samples were incubated in the CE instrument at 37 °C. An internal marker peptide (PSKD) was added to the CE samples to adjust for variation in injection volume and electroosmotic flow. The concentration of soluble peptide was determined from the corrected peak areas with reference to a standard curve.

Thioflavin T (ThT) Fluorescence Spectroscopy—ThT fluorescence was measured using a FLUOstar Optima fluorescence plate reader system (BMG Labtech). Equal volumes of peptide and ThT solution with or without Cu(II) were mixed. The final concentration of ThT was 20 μM in all experiments. Sample volume was 90 μl of reaction mixture and the plates were incubated at 37 °C. Blank samples with HEPES buffer and 20 μM ThT alone were analyzed to correct for background fluores-

cence by subtraction. The plate was shaken for 3 s prior to each measurement using 1-mm orbital shake.

Inductively Coupled Mass Spectrometry (ICP-MS)—ICP-MS investigations of the peptide aggregates were performed using a PE-SCIEX ELAN 6000 instrument (PerkinElmer Life Sciences). The peptide-Cu(II) samples were incubated at 37 °C and afterward centrifuged at $14,000 \times g$ for 1 h. The supernatant was removed and the precipitate was dissolved by addition of high-purity concentrated HNO_3. This solution was diluted with the 20 mM HEPES buffer prior to ICP-MS analysis. The total copper content in the re-dissolved aggregates was quantified with reference to a matrix-matched calibration curve. The concentration of Cu(II) in solution (free plus peptide-bound) was calculated by subtraction of the aggregate-bound Cu(II) from the total amount of Cu(II).

Atomic Force Microcopy (AFM)—For AFM investigations the peptide and peptide-Cu(II) samples were incubated at 37 °C. Aliquots of 20 μl from the incubation solution were applied onto polished silicon wafers modified by amino-silane at different times after incubation. The deposited material was carefully washed three times with 100 μl of water, and subsequently dried in a gentle stream of nitrogen. All images were obtained with a PSIA XE 150 microscope (Park Systems Inc.) in true non-contact mode. The resonance frequency was 300 kHz and the force constant was 40 newton m^{-1}. For each treatment a minimum of three locations were investigated.

Scanning Electron Microscopy (SEM)—Samples for SEM were incubated at 37 °C and applied on a silica wafer using the same procedure as in the AFM experiments. The wafers were sputter-coated with a ~10-nm thin gold layer prior to measurement to make the surface electrically conducting. Samples were examined in an Ultra55 scanning electron microscope (Carl Zeiss). An acceleration voltage of 3.00 kV and a 2-mm working distance were used. For each treatment a minimum of four locations were investigated.

Data Analysis and Model Comparison—Data analysis and fitting were carried out using GrapPad Prism 5.0 (GrapPad Software). Concentration-time (CE and ICP-MS data) and fluorescence-time profiles were fitted to four different models (supplemental Equations S1–S4). Model discrimination was carried out by visual comparison of the fits, the size of the SE of the fitted parameters, and by evaluation of the corrected Akaike's information criterion (AIC$_C$) (36). Further details are provided under supplemental Materials.

Numerical Simulations—Simulations of the suggested reaction pathways in Fig. 5 were performed by numerical integration of the corresponding differential equations using KinTek Explorer (37) (KinTek Corporation). Further details are provided under supplemental Materials.

RESULTS

Spontaneous Aβ Aggregation Kinetics—To study the effect of Cu(II) on the aggregation of Aβ$_{1-40}$, a kinetic model was established for the spontaneous aggregation of Aβ$_{1-40}$. This was done using CE to monitor the disappearance of soluble peptide (Fig. 1, *A* and *B*) and fluorescence spectroscopy to detect the concomitant appearance of aggregating ThT fluorescent species (Fig. 1C).

The peak representing soluble Aβ$_{1-40}$ was narrow and symmetrical in the CE analysis (Fig. 1A) demonstrating that the analyte was homogenous with respect to the charge-to-size ratio and thus most likely represents the peptide monomer. After an initial lag time the soluble Aβ$_{1-40}$ population started to decrease and had almost fully disappeared after >15 h (Fig. 1). A simple two-step autocatalytic model (nucleation followed by autocatalytic aggregation, supplemental Equation S1), that accounts well for published kinetic data in various studies of amyloidogenic proteins (38), fitted the CE data points adequately over a range of peptide concentrations (40–120 μM) (Fig. 1B, *inset*). The ThT data showed that the formation of fibrils could be described using the same two-step autocatalytic model with curves (Fig. 1C) that are mirror images of the CE data (Fig. 1B), and with rate constants of the same order of magnitude as the values estimated from the CE experiments (Table 1) and those previously determined for Aβ using this model (38). Thus, the two-step autocatalytic model was concluded to be a suitable model for the spontaneous aggregation of Aβ$_{1-40}$. In addition to the CE and ThT experiments with apo-Aβ$_{1-40}$, CE was used to follow the aggregation kinetics of Aβ$_{1-42}$ at pH 10.5 (40 and 60 μM, supplemental Fig. S1). The spontaneous aggregation of Aβ$_{1-42}$ could also be described by the two-step autocatalytic growth model (supplemental Fig. S2 and Table S1).

Cu(II) Affects the Aβ Aggregation in a Concentration-dependent Manner—Next, we studied the effect of Cu(II) on Aβ aggregation. There are conflicting reports on the Cu(II):Aβ binding stoichiometry (33, 39). Also, as noted by others (39), a physiological relevance of supraequimolar Cu(II):Aβ ratios is possible, because the concentration of Aβ in CSF is in the nanomolar range (40, 41), whereas the release of Cu(II) from neurons may reach micromolar levels in the extracellular space (19). Thus, three different Cu(II) concentrations (10, 40, and 200 μM) were chosen to reflect subequimolar (0.25:1), equimolar, and supra-equimolar (5:1) Cu(II):Aβ ratios.

In the presence of Cu(II), aggregation of Aβ$_{1-40}$ started instantaneously at all three Cu(II):Aβ ratios (Fig. 1B). This is in agreement with other studies (4, 5). The individual kinetic profiles, however, varied considerably depending on the molar ratios. At subequimolar Cu(II):Aβ ratios, the kinetic curves were similar to the profile of the apo form with the exception of an initial decrease of about 10 μM in soluble Aβ$_{1-40}$ as determined from the first CE measurement (~3 min after start of incubation, Fig. 1B, *blue trace*). This indicates that the added 10 μM Cu(II) immediately (<3 min) induced aggregation of an equimolar amount of Aβ$_{1-40}$ upon addition. The remaining soluble Aβ$_{1-40}$ followed the spontaneous aggregation pathway (the two-step autocatalytic mechanism) as illustrated by both the CE and ThT data (Fig. 1, *B* and *C*, and Table 1), indicating that the presence of aggregated Aβ-Cu did not influence the self-assembly process of the remaining peptide in solution. Note that the Aβ$_{1-40}$ aggregating instantly upon Cu(II) incubation, as detected by CE, do not result in an increase in ThT fluorescence, contrary to the subsequent aggregation of the apo Aβ$_{1-40}$. Thus the initially formed aggregates with Cu(II) had only minimal β-sheet structure.
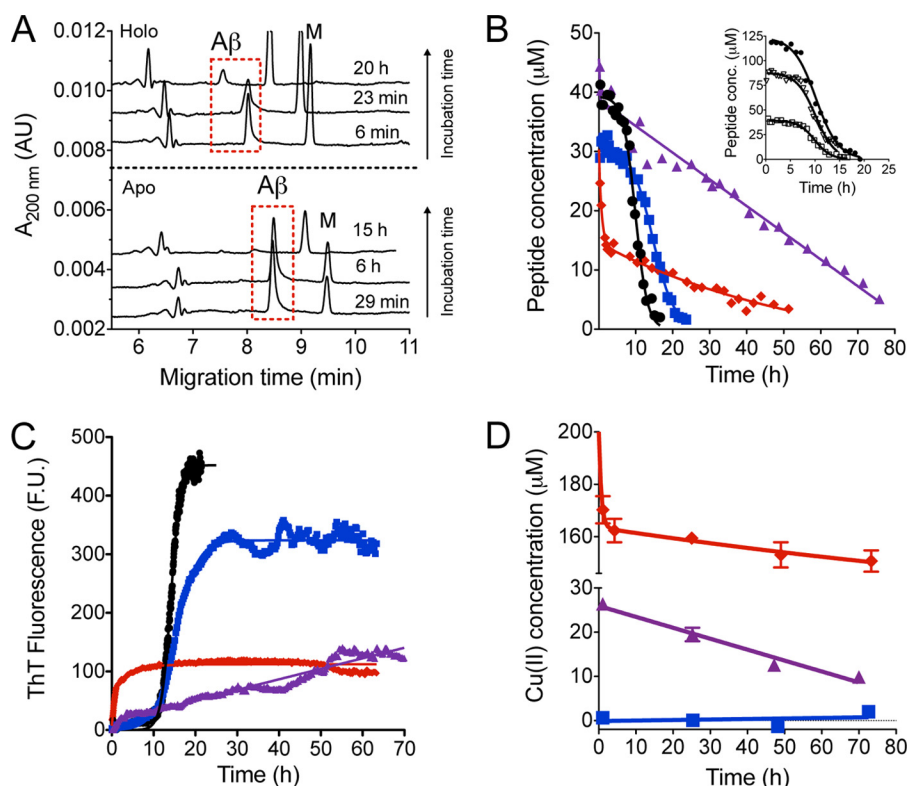
FIGURE 1. **Aggregation of 40 μM Aβ$_{1-40}$ in 20 mM HEPES (pH 7.4) and 37 °C.** *A*, electropherograms at various times after incubation showing the disappearance of soluble Aβ$_{1-40}$ due to spontaneous fibrillation (apo) and Cu(II)-induced aggregation (holo). A marker peptide (*M*) was added to the solution. *B*, disappearance kinetics of soluble Aβ$_{1-40}$ in the absence (●, *black*) and presence of 10 (■, *blue*), 40 (▲, *purple*), and 200 (◆, *red*) μM Cu(II). Data are fitted to supplemental Equation S1 (0 and 10 μM), supplemental Equation S2 (40 μM), and supplemental Equation S4 (200 μM). *Inset*, effect of Aβ$_{1-40}$ concentration on the spontaneous (*i.e.* in the absence of Cu(II)) fibrillation of the peptide. Initial Aβ$_{1-40}$ concentration is 40 (□), 85 (▽), and 120 μM (●, *black*). Data were fitted to a two-step autocatalytic mechanism (supplemental Equation S1). *C*, fibril formation kinetics of Aβ$_{1-40}$ from one ThT experiment in the absence (●, *black*) and presence of 10 (■, *blue*), 40 (▲, *purple*), and 200 μM (◆, *red*) Cu(II). *D*, disappearance kinetics of soluble Cu(II) determined from ICP-MS. 40 μM Aβ$_{1-40}$ was incubated with 10 (■, *blue*), 40 (▲, *purple*), and 200 μM (◆, *red*) Cu(II). Data points are mean ± S.D. (*n* = 3).

TABLE 1

Rate constants for the aggregation of Aβ$_{1-40}$ (40 μM) and added Cu(II) (10–200 μM), and formation of ThT-positive aggregates

The experiments were performed at 37 °C in 20 mM HEPES buffer with 100 mM NaCl (pH 7.4). Values are best-fitted values ± S.E. The range of the individual best fit is listed in brackets for k_1 in the two-phase autocatalytic (AC) model. *n* is the number of individual experiments. For the two-phase AC model k_1 is the rate constant of nucleation, and k_2 is the rate constant of fibril growth. For the linear function model, k_1 is the 0 order rate constant. For the bi-exponential model k_1 is the rate constant for the fast exponential term, and k_2 is the rate constant for the slow exponential term. For more details see the supplemental materials.

Cu(II):Aβ$_{1-40}$ ratio	Measured specie	Model	k_1	k_2
0	Aβ[a]	Two-phase AC[b] (*n* = 4)[c]	$(4.8 \times 10^{-9}–1.2 \times 10^{-6})$ s^{-1}	$(3.5 \pm 0.3) \times 10^{-6}$ μM^{-1} s^{-1}
0	Aggregates[d]	Two-phase AC[b] (*n* = 3)[c]	$(1.0 \times 10^{-9}–3.8 \times 10^{-5})$ s^{-1}	$(6.15 \pm 0.05) \times 10^{-6}$ μM^{-1} s^{-1}
0.25	Aβ[a]	Two-phase AC[b] (*n* = 3)[c]	$(2.7 \times 10^{-8}–9.0 \times 10^{-7})$ s^{-1}	$(2.8 \pm 0.2) \times 10^{-6}$ μM^{-1} s^{-1}
0.25	Aggregates[d]	Two-phase AC[b] (*n* = 3)[c]	$(7.7 \times 10^{-8}–1.1 \times 10^{-6})$ s^{-1}	$(2.75 \pm 0.03) \times 10^{-6}$ μM^{-1} s^{-1}
0.25	Copper[e]	Linear function[f] (*n* = 3)	n.s. ($p = 0.463$)[g]	
1	Aβ[a]	Linear function[f] (*n* = 4)[c]	$(1.2 \pm 0.3) \times 10^{-4}$ μM s^{-1}	
1	Copper[d]	Linear function[f] (*n* = 3)	$(6.8 \pm 0.7) \times 10^{-5}$ μM s^{-1}	
5	Aβ[a]	Biexponential[h] (*n* = 3)[c]	$(3.3 \pm 0.2) \times 10^{-4}$ s^{-1}	$(6.5 \pm 0.2) \times 10^{-6}$ s^{-1}
5	Aggregates[d]	Biexponential[h] (*n* = 3)[c]	$(5.8 \pm 0.5) \times 10^{-4}$ s^{-1}	$(7.7 \pm 0.2) \times 10^{-5}$ s^{-1}
5	Copper[e]	Biexponential[h] (*n* = 3)	$(4.3 \pm 2.0) \times 10^{-4}$ s^{-1}	$(4.0 \pm 2.0) \times 10^{-6}$ s^{-1}

[a] Detected with CE.
[b] Supplemental Equation S1.
[c] Global fit.
[d] Detected with ThT fluorescence spectroscopy.
[e] Detected with ICP-MS.
[f] Supplemental Equation S2.
[g] Statistical test for significantly non-zero slope.
[h] Supplemental Equation S4.

At equimolar Cu(II):Aβ ratios, the aggregation kinetics was surprisingly found to be much slower and soluble peptide was still detected after >70 h (Fig. 1*B*, *purple triangles*). After an initial decrease of ~5–15 μM in the concentration of soluble peptide (Fig. 1*B* and supplemental Fig. S3) the concentration of soluble Aβ$_{1-40}$ slowly decreased linearly with time. Similar kinetics was observed for the increase in ThT fluorescence (Fig.

1*C, purple trace*). The two-step autocatalytic model did not adequately describe this data set, which was best fitted by a linear function (supplemental Equation S2). This strongly suggests that different aggregation mechanisms were involved under subequimolar as compared with equimolar conditions. We suggest the existence of a relatively stable and soluble Aβ-Cu complex as previously proposed (42), because of the

slow aggregation kinetics of $A\beta_{1-40}$ at equimolar Cu(II):$A\beta_{1-40}$ ratios. The aggregation of this soluble complex becomes the rate-limiting step of the aggregation process.

At supraequimolar Cu(II):$A\beta_{1-40}$ ratios an initial fast decrease in the soluble peptide was observed within the first 2 h corresponding to ~65% aggregation of the peptide (Fig. 1, *A* and *B, red diamonds*, and supplemental Fig. S3). After the initial fast phase the disappearance rate of soluble $A\beta_{1-40}$ decreased and soluble peptide was still detected after >50 h (Fig. 1*B*). A similar pattern was seen for the aggregate formation kinetics measured by ThT fluorescence where an initial fast increase in the fluorescence intensity was observed during the first 1–2 h (Fig. 1*C, red trace,* and supplemental Fig. S3) followed by a relatively constant and stable fluorescence signal over the next 40–50 h. The soluble $A\beta_{1-40}$ remaining after 50 h was not susceptible to further Cu(II)-induced aggregation (supplemental Fig. S4). This indicates that the remaining soluble peptide was already fully loaded with Cu(II), and that the aggregation of a soluble $A\beta$-Cu_y complex is rate-limiting as observed under equimolar conditions. Recently it has been shown that Cu(II) decreases the hydrophobic exposed protein surfaces of $A\beta_{1-40}$ when added in supraequimolar ratios (43), which may explain the observed increased solubility of the $A\beta$-Cu complex.

Both the peptide loss (CE data) and the aggregation formation kinetics (ThT data) at supraequimolar ratios were best fitted to a sum of two exponential functions (supplemental Equation S4). However, upon closer comparison of the CE and ThT profiles (Fig. 1, *B* and *C, red traces*) it was evident that there were some differences with respect to the slower phase (Table 1). The slow loss of peptide seen after 3–4 h using CE did not give rise to an increase in ThT fluorescence. This again suggests that there were structural differences between the initially formed aggregates and the aggregates slowly formed during the second phase. The structural difference is most likely reflected in the amount of β-sheet present in the aggregates. Furthermore, the initial decrease in soluble peptide occurred in parallel with the increase in ThT fluorescence. This suggests that the aggregates formed initially within the first hours at supraequimolar Cu(II):$A\beta$ ratios are structurally different from the aggregates that were formed initially at the subequimolar ratio, because an initial increase in ThT fluorescence were not observed under these conditions, despite a decrease in soluble peptide, see above (Fig. 1, *B* and *C, blue traces*).

Moreover, CE studies were performed to study the influence of Cu(II) on the aggregation of $A\beta_{1-42}$ using the same metal: peptide ratios. Like the case with $A\beta_{1-40}$, the Cu(II):$A\beta_{1-42}$ ratio also influenced the aggregation kinetics of Cu-$A\beta_{1-42}$ and different kinetic scenarios were also observed depending on the Cu(II):$A\beta_{1-42}$ ratio that all differed from the spontaneous aggregation of $A\beta_{1-42}$ (supplemental Figs. S1 and S2, and Table S1). It should be noted that the apparent aggregation kinetics of Cu-$A\beta_{1-42}$ was not identical to the aggregation kinetics seen for Cu-$A\beta_{1-40}$ at the same metal:petide ratios. However, due to the difference in experimental conditions (*e.g.* pH), a detailed comparison of the kinetic profiles of $A\beta_{1-40}$ and $A\beta_{1-42}$ was not possible. The qualitative observation that the Cu(II)-induced aggregation kinetics and hence aggregation mechanism was dependent on the metal:peptide ratio for both $A\beta_{1-40}$ and

$A\beta_{1-42}$ was consistent, however, and suggests that the propensity to enter multiple aggregation pathways is an inherent property of $A\beta$ peptides. In summary, both the CE and ThT experiments showed that the rate of loss of soluble peptide and the emergence of ThT-positive aggregates strongly depend on the metal:peptide ratio, and that three different Cu(II)-induced aggregation pathways exist depending on this ratio.

Cu(II) Binds to Aβ Aggregates in Different Ratios—To examine the disappearance kinetics of soluble Cu(II), we used ICP-MS to measure the copper content in isolated $A\beta$-Cu aggregates (Fig. 1*D*). At subequimolar Cu(II):$A\beta$ ratios all the copper was bound in the aggregated material ($c_{Cu(II)}$ in the redissolved aggregates was 10 ± 1 μM, mean $\pm$ S.D., $n = 12$), *i.e.* all Cu(II) had disappeared from solution at the first ICP-MS measurement (~1 h, Fig. 1*D, blue squares*). This confirms that the 10 μM $A\beta_{1-40}$ that instantaneously aggregates upon addition of 10 μM Cu(II) in the CE experiments (Fig. 1*B, blue squares*) contained copper in a 1:1 stoichiometry. This is compatible with the notion that $A\beta_{1-40}$ has one high affinity Cu(II)-binding site (33, 39) and that Cu(II) is bound to the aggregates in a 1:1 ratio (32, 44). In addition, ICP-MS data showed that the copper stays bound to the aggregates during the entire time course of the experiment (72 h).

At equimolar ratios, ~26 μM Cu(II) remained in solution after the first measurement (Fig. 1*D, purple triangles*). This also corresponds well with the observed initial decrease in soluble peptide (Fig. 1*B, purple triangles,* and supplemental Fig. S3) confirming the 1:1 stoichiometry of the $A\beta$-Cu(II) aggregates. Hereafter, the concentration of soluble Cu(II) decreased at a constant rate that was comparable with the decrease in soluble peptide (Table 1). This supports our previous notion that aggregation of the soluble $A\beta$-Cu(II) complex is a rate-limiting step, see above, and shows that the complex retained its metal:peptide stoichiometry upon aggregation.

At supra-equimolar ratios an initial fast decrease in the soluble Cu(II) concentration was seen followed by a slower second phase (Fig. 1*D, red diamonds*). This two-phase kinetics also agrees with the kinetics seen in the CE and ThT experiments (Table 1). This confirms that Cu(II) was bound to $A\beta_{1-40}$ upon aggregation. The analysis of the peptide and Cu(II) aggregation kinetics at the supra-equimolar concentration shows that copper was bound to the $A\beta$ aggregates in a constant molar metal: peptide ratio of 1.4 ± 0.1 (mean $\pm$ S.D., $n = 15$) throughout the time course of the experiment. This implies that a second Cu(II)-binding site is partially occupied in the $A\beta$-Cu(II) aggregates at this metal:peptide ratio, and this could be a reason for the apparent structural differences in the aggregates as detected by the ThT fluorescence. Conclusively, the ICP-MS data showed that copper co-aggregates with $A\beta$ in a ~1:1 stoichiometry at Cu(II):$A\beta$ ratios ≤ 1 and in a 1.4 ratio at Cu(II):$A\beta$ ratios >1.

Cu(II) Promotes Time-dependent Changes in the Morphology of Aggregates—The studies of peptide disappearance and aggregate formation kinetics demonstrated that Cu(II) has a profound influence on the aggregation kinetics of $A\beta_{1-40}$. Also, from the ThT experiments it is evident that the fluorescence signal itself is affected by the amount of Cu(II) present because a decrease in the plateau intensity was seen with increasing
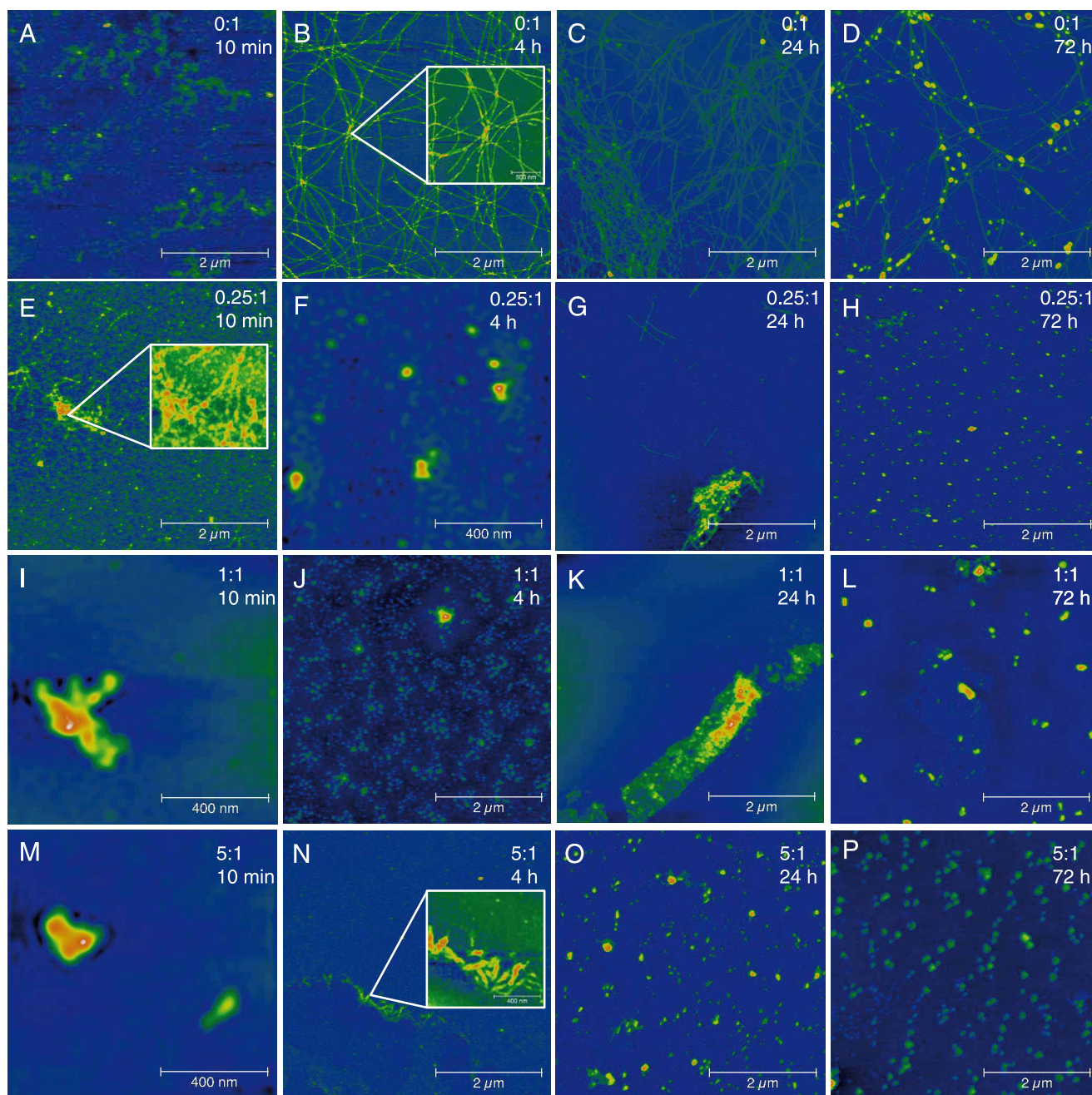
FIGURE 2. **AFM pictures of the aggregates formed from 40 μM Aβ_{1-40} solution at different metal:peptide ratios and incubation times as indicated.** Fibrils were not detected initially in the absence of Cu(II) (*A*). Fibrils were observed in the absence of Cu(II) after 4 h (*B*). Spherical aggregates were observed on top of fibrils after 24 and 72 h (*C* and *D*). Amorphous aggregates were observed in the presence of Cu(II) (*E–P*). The aggregates showed some fibrillar structure (*E* and *G*). Fibrils were not detected at equimolar and supra-equimolar Cu(II) concentrations (*I–P*). The experimental conditions were the same as described in the legend to Fig. 1.

Cu(II) (Fig. 1*C*). A study on Aβ_{1-42} reports that the ThT fluorescence intensity after a 6-h incubation at 37 °C with 5 molar eq of Cu(II) is reduced to about 20% of the intensity without Cu(II) (26). This reduction is identical to our ThT results with excess Cu(II), where an 80% reduction in intensity was observed (Fig. 1*C*, *red trace*). However, contrary to the previous study where it is concluded that the reduction in ThT signal is due to Cu(II) inhibiting the aggregation of Aβ_{1-42} (26), our CE results clearly indicate that Cu(II) induced pronounced aggregation of Aβ in the first hours after incubation. Thus, the relative decrease in ThT fluorescence intensity in the presence of Cu(II)

most likely reflects a decrease in the number of ThT binding sites (45), *i.e.* a decrease in the β-sheet content of the peptide aggregates as compared with the situation in the absence of Cu(II) (46). Additionally, Cu(II)-dependent quenching also takes place especially in the presence of excess Cu(II). The above findings suggest Cu(II)-dependent differences in aggregate structure. Earlier reports have suggested that the amyloidogenic characteristics of Cu(II)-treated fibrils is decreased (15, 17).

The time-specific morphology of the fibrils and aggregates was studied using AFM (Fig. 2). Without Cu(II), fibrils or aggre-

gates were not detected initially (Fig. 2*A*), which is in good agreement with the observed kinetics where a lag phase of ~3–10 h was observed (Fig. 1, *B* and *C*). This also verifies that only minimal amounts of insoluble aggregated Aβ are initially present in the filtered and centrifuged peptide solutions. Small fibrils were observed after 4 h (Fig. 2*B*). These fibrils continued to grow in length and number until 24 h where they reached a length of ~2–3 μm and a height of 10–20 nm (Fig. 2*C*). This agrees with the observed kinetics, where all soluble peptide disappeared (Fig. 1*B*) and a maximum ThT fluorescence was observed after about 20 h (Fig. 1*C*). The fibrils were unbranched but intertwined and in some cases appeared to have a common nucleus from which multiple threads were sprouting (Fig. 2*B, inset*). After prolonged incubation the number of fibrils appeared to decrease (Fig. 2*D*). Instead, small spherical aggregates were observed ranging from 10 to 100 nm in diameter lying on top of the formed fibrils like pearls on a string. These aggregates resemble previously reported early oligomeric assemblies of Aβ$_{1-40}$ (47), and were also morphologically indistinguishable from the Cu(II)-induced aggregate species observed in this study (see below) and elsewhere (15). However, the presence of spherical assemblies subsequent to fibrillation in the absence of metal ions has to our knowledge not previously been reported, although they have been observed prior to fibril formation (48). Transformation of fibrils into spherical aggregates over time is consistent with the observation that the ThT fluorescence slowly decreases after having reached an initial plateau (data not shown).

At a 0.25:1 molar metal:peptide ratio amorphous aggregates and a few fibrillar structures were seen immediately upon addition of Cu(II) (Fig. 2*E*). This corresponds well with the kinetics observed in the CE analyses (Fig. 1*B, black circles*) where a decrease in the concentration of soluble peptide was detected immediately after incubation. Although the aggregates displayed some fibrillar characteristics (Fig. 2*E, inset*), they were generally amorphous in nature (Fig. 2*F*). After 24 h, individual fibrils were observed but amorphous aggregates still predominated (Fig. 2*G*). The formed aggregates had some amyloidogenic properties because a relatively high signal was attained in the ThT assay of these solutions. After 72 h fibrils were completely absent and only small spherical aggregates with a diameter of ~40–60 nm were detected (Fig. 2*H*).

Incubation of Aβ$_{1-40}$ with equimolar and supra-equimolar concentrations of Cu(II) led to immediate formation of large amorphous aggregates without any apparent fibrillar morphology as detected by AFM in accordance with earlier studies (15, 49, 50). At the 1:1 ratio the aggregates increased in size (from about 100–400 nm to >1 μm) until 24 h of incubation (Fig. 2, *I–K*). Afterward the aggregates diminished in size but increased in numbers (Fig. 2*L*) in accord with the decrease in soluble peptide seen in the CE experiments (Fig. 1*B*). Fibrils were not detected by AFM at any time point at the 1:1 metal:peptide ratio. However, the formed aggregates could have some amyloidogenic properties because a steady increase in the ThT signal was observed in parallel with the disappearance kinetics of soluble peptide (Fig. 1, *B* and *C*). It should be noted that the increase in ThT intensity could be independent on the presence of any form of fibrillar structures (51).

At the 5:1 metal:peptide ratio large aggregates were seen immediately upon Cu(II) addition (Fig. 2*M*). The aggregates were similar in size to the aggregates formed at the 1:1 ratio. After ~4 h, aggregates were seen possessing some fibrillar characteristics (Fig. 2*N, inset*), and this could explain the rapid increase in ThT fluorescence observed during the first 5–10 h at this concentration level (Fig. 1*C, red trace*). At 24 and 72 h only small spherical aggregates were found (Fig. 2, *O* and *P*) resembling those seen at 72 h at 0.25:1 and 1:1 Cu(II):Aβ ratios (Fig. 2, *H* and *L*).

We also examined the incubated peptide solutions using SEM, to gain complementary information about the aggregate morphology (supplemental Fig. S5). Overall, the morphology and evolution of fibrils and aggregates detected by SEM were identical to what was observed with AFM. The only difference was that in the SEM the Cu(II)-induced amorphous aggregates still displayed a relatively high degree of fibril-like structure with fibrils laterally aggregated in bundles. This is consistent with previous studies using TEM (39, 52) and would also explain the detection of an increase in ThT fluorescence even in the presence of Cu(II). The presence of this fibrillar structure may not be so easily discerned on an aggregate background using AFM.

In summary, AFM and SEM document distinct aggregate morphologies depending on the Cu(II):peptide ratio and the incubation time. The insoluble phase is strikingly dynamic changing from fibrillar to a mixture of fibrillar and spherical structures. Cu(II) consistently induced aggregates with minor or no discernable fibrillar structure. Also, in all AFM experiments small spherical aggregates appeared after prolonged incubation (72 h) possibly indicating a common end point for the aggregation process. The results suggest that fibrillation and ThT fluorescence are not necessarily tightly coupled, *i.e.* other aggregates than fibrillar amyloid assemblies may exhibit increases in ThT fluorescence.

Peptide Length Determines Aggregational Propensity—The short peptide variants Aβ$_{1-16}$ and Aβ$_{1-28}$ were studied to investigate the influence of the peptide length on the Cu(II)-induced aggregation, and to gain general insight into the molecular mechanism of the Cu(II)-induced aggregation. The short variants both contained the three proposed Cu(II)-binding histidines and are known to bind Cu(II) in a coordination sphere with an affinity similar to the full-length peptide (52–55). A major difference between the two variants is that Aβ$_{1-28}$ forms fibrils (56, 57), whereas Aβ$_{1-16}$ apparently does not (58) due to the lack of the critical hydrophobic LVFFA sequence needed for self-assembly (59). The spontaneous and Cu(II)-induced aggregation of Aβ$_{1-16}$ seemed to be very similar (Fig. 3*A*). Both the apo and holo forms slowly aggregated linearly at the same rate (Table 2) suggesting that Cu(II) does not influence the aggregation kinetics of Aβ$_{1-16}$. This was also reported previously (42), although on a much shorter time scale (2 h incubation). As seen, ~50% of the peptide had aggregated after 14 days but an increase in ThT fluorescence were not observed during this time (data not shown). Hence, the aggregates did not contain any β-sheet structure and were most likely non-fibrillar in nature as expected.
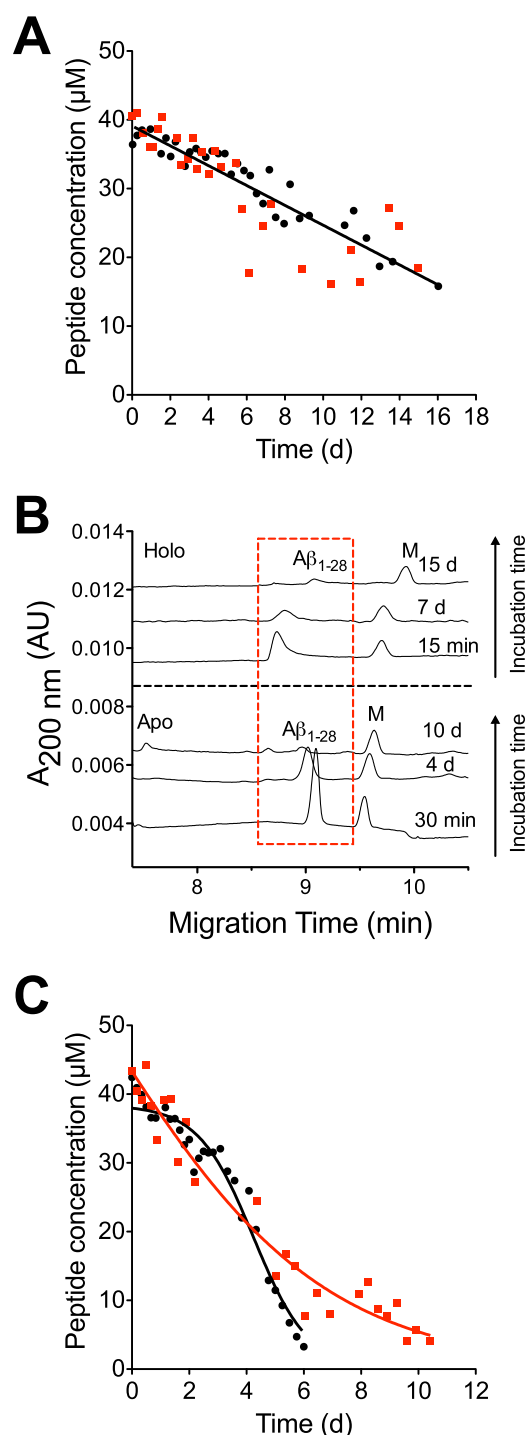
FIGURE 3. **Aggregation of 40 μM Aβ$_{1-16}$ and Aβ$_{1-28}$ showing the effect of peptide length for the Cu(II)-induced aggregation.** *A*, decrease in soluble Aβ$_{1-16}$ in the absence (●, *black*) and presence of 200 μM (■, *red*) Cu(II). Data points are fitted to supplemental Equation S2. *B*, decrease in soluble Aβ$_{1-28}$ in the absence (●, *black*) and presence of 200 μM (■, *red*) Cu(II). Data points are globally fitted to supplemental Equations S1 or S3. *C*, electropherograms at various times (*top*) with and (*bottom*) without Cu(II) showing the disappearance of soluble Aβ$_{1-28}$ due to aggregation. A marker peptide (*M*) is added to the solution. The experimental conditions were the same as described in the legend to Fig. 1.

Next, the aggregation kinetics of Aβ$_{1-28}$ was monitored with and without Cu(II). CE showed that the peak shape of Aβ$_{1-28}$ and peak appearance time were altered by the presence of Cu(II) (Fig. 3*B*). Without Cu(II) the peptide peak was sharp and

symmetrical, whereas it was broader and tailing in the presence of Cu(II). This was most likely caused by dissociation of Cu(II) from the peptide when the sample was injected into the electrophoresis buffer and electrophoresis was applied. Results based on stopped-flow spectroscopy (27) show that the dissociation rate constant of Cu(II) from the Aβ-Cu(II) complex is ~0.1 s^{-1} meaning that the complex had completely dissociated at the time (about 9 min) of detection (60).

We found that the spontaneous aggregation of Aβ$_{1-28}$ followed a sigmoidal curve shape that is compatible with the two-step autocatalytic model (Fig. 3*C*). The rate constant for the autocatalytic step of Aβ$_{1-28}$ aggregation is approximately an order of magnitude smaller than for Aβ$_{1-40}$ suggesting that the formation of aggregates is less favorable for the smaller peptide (Table 2). Surprisingly, as with the 1–16 variant, an increase in ThT fluorescence was not observed (data not shown) even though the sigmoidal aggregation kinetic profile suggests that the aggregation follows a model, which results in formation of fibrils. This may be because the peptide concentration (40 μM) was too low to yield a discernable signal as was reported by Shen *et al.* (57) where concentrations of ≥120 μM yielded an increase in ThT fluorescence after 24 h of incubation.

When Aβ$_{1-28}$ was incubated with supra-equimolar Cu(II), concentration changes in the aggregation profile were observed. The two-step autocatalytic model could not describe the data, and the decrease in soluble peptide appeared to follow a single exponential decay (Fig. 3*C*). Also, as seen with the holo forms of Aβ$_{1-40}$ there was a tendency for a faster aggregation initially, followed by a higher stability of the soluble peptide, although it was less evident than for Aβ$_{1-40}$. However, as seen in Fig. 3*C* soluble Aβ$_{1-28}$ was still present after 11 days when incubated with Cu(II), whereas it had fully disappeared after 6 days in the absence of Cu(II). This indicates that the Cu(II) binding to Aβ$_{1-28}$ stabilizes a metal-peptide complex that has a slower rate of aggregation exactly as was found for Cu-Aβ$_{1-40}$. To sum up, the experiments with Aβ$_{1-16}$ and Aβ$_{1-28}$ showed that other amino residues than the Cu(II) binding His residues are of importance in the Cu(II)-induced aggregation.

Model for Aβ Aggregation in the Absence and Presence of Cu(II)—A mechanistic model is depicted in Fig. 4, which describes the influence of Cu(II) on the aggregation of Aβ$_{1-40}$ including the observation that the aggregates are structurally dynamic and undergo time-dependent morphological transformations. The presented model shows that when Cu(II) is not present the aggregation of Aβ$_{1-40}$ follows a mechanism that can be described by the two-step autocatalytic model with the formation of ThT-positive fibrils. When Cu(II) is present it rapidly binds to Aβ forming a soluble 1:1 Aβ-Cu(II) complex. This complex either aggregates quickly (within minutes) or remains soluble over a long period of time (hours-days) depending on the metal:peptide ratio, indicating the existence of multiple aggregation pathways and/or limiting steps.

Kinetic profiles for Aβ and Cu(II) based on numerical simulations of the model are largely compatible with the experimental data (Fig. 5 and supplemental Table S2) and with the results of this study as well as previous reports (31, 39, 61). The ThT profiles were not simulated because the ThT fluorescence intensity was influenced by the addition of Cu(II). Thus differ-

Cu(II)-dependent Aβ Aggregation Pathways

TABLE 2

Rate constants for the aggregation of Aβ$_{1-16}$ and Aβ$_{1-28}$ (40 μM) with and without the addition of Cu(II) (200 μM)

The experiments were performed at 37 °C in 20 mM HEPES buffer with 100 mM NaCl (pH 7.4). Values are best-fitted values ± S.E. n is the number of individual experiments. For the two-phase AC model k_1 is the rate constant of nucleation, and k_2 is the rate constant of fibril growth. For the linear function model, k_1 is the 0 order rate constant. For the monoexponential model k_1 is the rate constant for the exponential term. For more details see the supplemental materials.

System	Model	k_1	k_2
Aβ$_{1-16}$	Linear function[a] ($n = 4$)[b]	$(1.78 \pm 0.07) \times 10^{-5}$ μM s^{-1}	
Aβ$_{1-16}$ + Cu(II)	Linear function[a] ($n = 4$)[b]	$(1.97 \pm 0.01) \times 10^{-5}$ μM s^{-1}	
Aβ$_{1-28}$	Two-phase AC[c] ($n = 4$)[b]	$(1.7 \pm 0.3) \times 10^{-7}$ s^{-1}	$(3.0 \pm 0.2) \times 10^{-7}$ μM^{-1} s^{-1}
Aβ$_{1-28}$ + Cu(II)	Monoexponential[d] ($n = 4$)[b]	$(2.0 \pm 0.8) \times 10^{-7}$ s^{-1}	

[a] Supplemental Equation S2.
[b] Global fit.
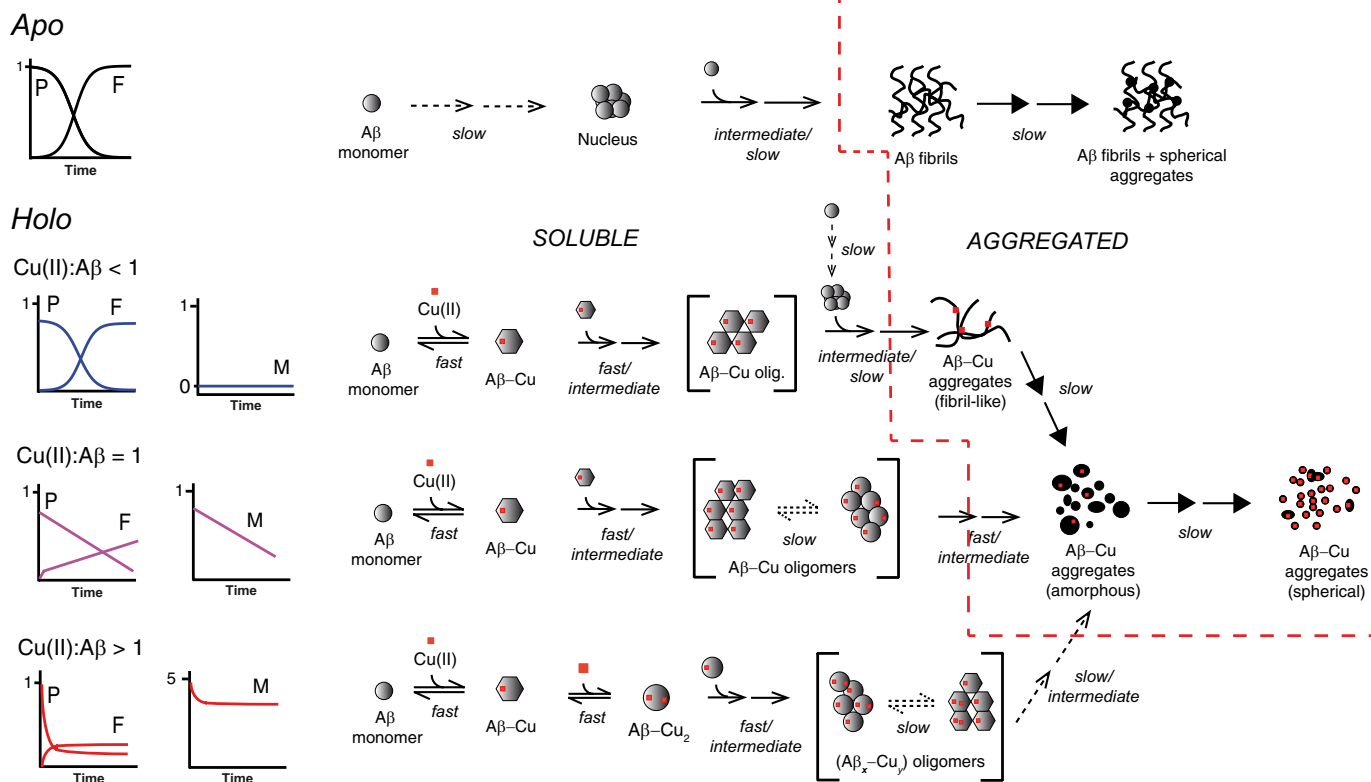[c] Supplemental Equation S1.
[d] Supplemental Equation S3.

FIGURE 4. **Mechanistic model for the Cu(II)-induced aggregation of Aβ$_{1-40}$.** Different aggregation pathways prevail depending on the metal:peptide ratio (M:P). *Apo*, Aβ aggregation and fibril formation follows a two-step autocatalytic model. *M:P < 1*, fast aggregation of equimolar Aβ and Cu(II). Remaining Aβ follows a two-step autocatalytic model. *M = P*, instantaneous aggregation of Aβ-Cu, followed by slow linear decrease in soluble Aβ and Cu(II), and linear increase in ThT fluorescence caused by formation of a stable and soluble Aβ-Cu intermediate. *M > P*, initial fast aggregation of Aβ and Cu(II) followed by slower aggregation. The Cu(II):Aβ ratio in (Aβ$_x$Cu$_y$)-oligomers and -aggregates are >1, *i.e.* y > x. Spherical Aβ-Cu aggregates constitute a common morphological end point in the presence of Cu(II). Soluble peptide disappearance (CE, *P*), soluble Cu(II) disappearance (ICP-MS, *M*), and aggregate formation (ThT-fluorescence, *F*) kinetic curves are also depicted schematically for each pathway. The peptide and metal curves are normalized to the initial Aβ concentration (40 μM). ThT fluorescence is normalized to the plateau level of apo-Aβ. Note that the Cu:Aβ ratio in the aggregates is not depicted quantitatively, and the color of the curves matches the corresponding curves in Fig. 1, *B–D*. The time scale of the different reaction steps are specified and divided into *fast* (millisecond to second time scale), *intermediate* (second to minute time scale), and *slow* (hour to day time scale). *Broken lines* in *reaction arrows* indicate a rate-limiting step. *Successive arrows* indicate multiple reactions steps. *Arrows with solid head* ($\rightarrow$) indicates morphological changes of aggregates. *Brackets* indicate the co-existence of several conformations in dynamic equilibrium. The *broken red line* separates the soluble and aggregates species. Not all possible species are explicitly depicted. *P*, soluble peptide (Aβ); *F*, ThT fluorescence; *M*, soluble metal (copper).

ent types of Aβ-Cu(II) aggregates are likely to have different ThT fluorescence responses, and it would not be possible to determine the fluorescence contribution of the individual species based on our studies. The model for the spontaneous aggregation, *i.e.* the two-step autocatalytic model (supplemental Equation S1) used rate constants based on the experimental data (Table 1). The simulated profiles justify that our model and proposed rate-limiting steps may provide kinetic profiles that are comparable with those obtained in the study (Figs. 1 and 5).

DISCUSSION

This study shows that Cu(II) has a great influence on the kinetics, aggregate morphology, and aggregate dynamics of polymeric Aβ in accordance with previous studies (5, 26, 42, 61). The metal:peptide ratio was found to be very important in this respect, which is also supported by previous studies (15, 49, 50). Unlike previous studies, however, this study is based on the combined kinetic analysis of both the loss of soluble peptide, aggregate/fibril growth, the aggregation of
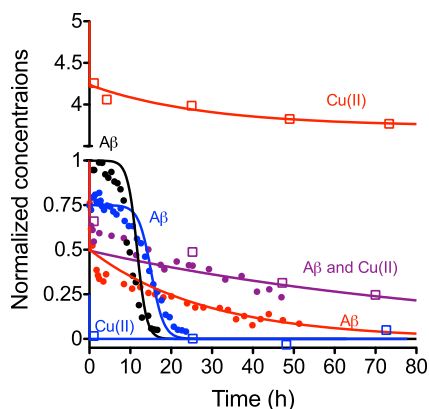
FIGURE 5. **Simulation of the concentrations of soluble Aβ and Cu(II) upon incubation.** The simulated curves are based on numerical integration of the differential equations and conditions (rate constants and concentrations) presented in supplemental Table S2. Experimental data for CE (*circles*) and ICP-MS (*open squares*) are superimposed on the simulated pair of curves for each condition. Data are taken from both Fig. 1 and supplemental Fig. S1. Concentrations for both Aβ and Cu(II) are normalized to the starting concentration of Aβ (40 μM). Color code: *black*, no Cu(II); *blue*, Cu(II):Aβ = 0.25; *purple*, Cu(II):Aβ = 1; *red*, Cu(II):Aβ = 5.

peptide-bound Cu(II), and the morphology of the formed aggregates. This approach allows a more rigorous analysis of kinetic data and enables us to probe deeper into the underlying Cu(II)-induced aggregation mechanisms. Most importantly, we here report for the first time that at least three distinct Cu(II)-induced aggregation scenarios exist. The three scenarios were all different from the sigmoid fibrillation kinetics seen for apo-Aβ and each one was dependent on the Cu(II):Aβ ratio. We found that Cu(II) both promoted and inhibited Aβ aggregation depending on both the metal:peptide ratio and the time of incubation as seen at supra-stoichiometric Cu(II) concentrations. This may provide an explanation for some of the contradicting reports in the literature on this subject. The discovery of distinct Cu(II)-dependent aggregation pathways suggests that future cytotoxicity studies need to take these aggregation mechanisms into account.

Recently, it has been proposed that the metal-induced aggregation of Aβ proceeds via building blocks of metal-Aβ and that the formation of a $Aβ_2$-metal$_2$ dimer is the rate-limiting step in the aggregation mechanism (31, 44). Although such a mechanism may account for some of the kinetic profiles that were observed in this study, it is not sufficient for a complete description at all concentration levels. Especially intriguing is the fact that the $Aβ_{1-40}$ samples containing equimolar concentrations of Cu(II) behave very differently from samples at both the sub- and supra-equimolar Cu(II) concentrations. Uniquely, equimolar conditions exhibit decreased initial metal-induced $Aβ_{1-40}$ aggregation and a slow constant disappearance rate of both $Aβ_{1-40}$ and Cu(II). An explanation could be that several conformations of the soluble Cu-Aβ complex exist (42, 58), and that the conformational equilibrium of this complex is affected by the metal:peptide ratio (16, 23, 39). EPR (62–64) and stopped-flow fluorescence experiments (27) with Aβ and Cu(II) confirm the co-existence of at least two different Aβ-Cu conformations at neutral pH. The difference, especially in the initial part of the kinetic curve between the aggregation experiments conducted at equimolar and supra-equimolar Cu(II) concentrations, could then be a direct consequence of a conformational equilibrium shift in the Aβ-Cu(II) complex, possibly involving the second binding site at the supra-equimolar Cu(II) concentration, because we here found that the metal:peptide stoichiometry in the aggregates was 1.4. This means that the dual effect of Cu(II) on the aggregation kinetics is most likely directly linked to the different Cu(II) coordination environments in Aβ (31, 65).

The experiments with $Aβ_{1-16}$ and $Aβ_{1-28}$ showed that the ability of Cu(II) to affect the aggregation kinetics is closely related to the spontaneous aggregation mechanism. We observed that only when the spontaneous aggregation followed a two-step autocatalytic mechanism ($Aβ_{1-28}$ and $Aβ_{1-40}$) did Cu(II) affect the aggregation kinetics. This suggests that Cu(II) shifts the Aβ aggregation pathway from a fibrillar route to a non-fribillar route, which would also be in accordance with the morphological results and other studies (39, 44). This effect is most likely not solely related to the Cu(II)-binding His residues, because Cu(II) did not affect the aggregation of $Aβ_{1-16}$. Thus, other factors, *e.g.* the chemistry of the peptide backbone or non-specific binding to some of the amino acids as suggested for human muscle acylphosphatase (66), could be of importance.

The schematic mechanistic model presented in Fig. 4 indicates that the presence of a slow-aggregating soluble Aβ-Cu(II) oligomer could act as a rate-limiting step for the overall aggregation process. This could be important for understanding the Aβ-Cu(II)-mediated neurotoxicity in Alzheimer disease as it has been suggested that it is a soluble form of Cu(II)-Aβ, which exerts the Cu(II)-mediated neurotoxicity, most likely through the generation of reactive oxygen species (14, 16, 35). Also, observations that Aβ-Cu(II) is only neurotoxic at Cu(II):Aβ ratios ≥1 with the 1:1 ratio being the most toxic (15, 16) is in agreement with the stabilizing effect of equimolar Cu(II) concentrations on the soluble Aβ species. Thus, compounds that can modulate or shift the equilibrium of the Aβ-Cu(II) complex to a less stable conformation or toward a non-toxic aggregated state could be a new therapeutic strategy for treating AD. Here it should be mentioned that a recent study showed, contrary to the previous reports, that it is the substoichiometric Cu(II) concentrations that are most cytotoxic, whereas an equimolar Cu(II) concentration does not increase Aβ cytotoxicity, and supra-stoichiometric Cu(II) concentrations reduce cytotoxicity (24).

We point out that the presented model, like any model, represents a simplified depiction of the possible events. Especially important for therapeutic applications is the fact that not all possible soluble and hence potentially toxic species are explicitly depicted. This is illustrated by the oligomerization processes for Aβ-Cu(II) (PM in supplemental Table S2) and Aβ-Cu$_2$ (PMM in supplemental Table S2) resulting in oligomeric Aβ-Cu(II) species (C and C1 in supplemental Table S2). These steps are reduced to one overall (fast) step, because they are not assumed to be rate-limiting (Fig. 4). In this respect it is noted that the oligomerization of actin and tubulin has been reported (67) to be on the order of $0.5–10 \times 10^6$ M^{-1} s^{-1} and $10^2–10^4$ times larger than the lower limit for the rate constants

for the oligomerization processes used to simulate the profiles shown in Fig. 5.

Moreover, the presented model is based on *in vitro* data obtained in a simplified system consisting only of peptides, ions, and buffers. *In vivo* many factors, *e.g.* other proteins and small peptides, could possibly affect the Cu^{2+}-induced aggregation of Aβ. In this connection an interesting protein is metallothionein-3, which has the ability to exchange Cu(II) with Zn(II). A recent study shows that this could be an important factor in the Aβ-Cu(II)-mediated cytotoxicity (13). Valuable additions to our model would be the implementation of kinetic aggregate size (*e.g.* size exclusion chromatography) and structural studies (*e.g.* circular dichroism or NMR) to gain further insight in the structure-function relationship of the Cu(II)-induced Aβ oligomerization and aggregation.

Finally, we note that the model presented in Fig. 4 address the *extracellular* interaction between Cu(II) and Aβ. Studies suggest that accumulation of intracellular Aβ is also implicated in the development of AD (68, 69) (reviewed in Ref. 70). Thus, it is possible that intracellular Cu could also play a role in this accumulation, although the oligomerization mechanism would most likely differ from the extracellular scenario due to the reductive intracellular environment, and the presence of cellular components. Nonetheless, the presented model provides novel insight in the underlying Cu(II)-induced aggregation mechanism of Aβ, and offers an explanation for the different aggregation scenarios observed in this study.

In addition to the implications for understanding AD it is increasingly recognized that several other amyloidogenic proteins associated with clinical important amyloidosis, *e.g.* $β_2$-microglobulin (dialysis-related amyloidosis) (71), prion protein (spongiform encephalopathies) (72), and α-synuclein (Parkinson disease) (73), may bind metal ions with modulation of their aggregation pathway as a consequence. Hence it is plausible that at least some of these proteins could share identical or similar metal-induced aggregation mechanisms and/or pathological pathways (65), and that the model presented in this study can serve as a template in the search for a unified understanding of mechanisms of amyloidogenicity.

REFERENCES

1. Hardy, J., and Selkoe, D. J. (2002) *Science* **297,** 353–356
2. Masters, C. L., Multhaup, G., Simms, G., Pottgiesser, J., Martins, R. N., and Beyreuther, K. (1985) *EMBO J.* **4,** 2757–2763
3. Lovell, M. A., Robertson, J. D., Teesdale, W. J., Campbell, J. L., and Markesbery, W. R. (1998) *J. Neurol. Sci.* **158,** 47–52
4. Bush, A. I., Pettingell, W. H., Multhaup, G., d Paradis, M., Vonsattel, J. P., Gusella, J. F., Beyreuther, K., Masters, C. L., and Tanzi, R. E. (1994) *Science* **265,** 1464–1467
5. Atwood, C. S., Moir, R. D., Huang, X., Scarpa, R. C., Bacarra, N. M., Romano, D. M., Hartshorn, M. A., Tanzi, R. E., and Bush, A. I. (1998) *J. Biol. Chem.* **273,** 12817–12826
6. Adlard, P. A., and Bush, A. I. (2006) *J. Alzheimers Dis.* **10,** 145–163
7. Barnham, K. J., and Bush, A. I. (2008) *Curr. Opin. Chem. Biol.* **12,** 222–228
8. Roychaudhuri, R., Yang, M., Hoshi, M. M., and Teplow, D. B. (2009) *J. Biol. Chem.* **284,** 4749–4753
9. Pimplikar, S. W., Nixon, R. A., Robakis, N. K., Shen, J., and Tsai, L. H. (2010) *J. Neurosci.* **30,** 14946–14954
10. Cuajungco, M. P., Goldstein, L. E., Nunomura, A., Smith, M. A., Lim, J. T., Atwood, C. S., Huang, X., Farrag, Y. W., Perry, G., and Bush, A. I. (2000) *J. Biol. Chem.* **275,** 19439–19442
11. Lovell, M. A., Xie, C., and Markesbery, W. R. (1999) *Brain Res.* **823,** 88–95
12. Huang, X., Cuajungco, M. P., Atwood, C. S., Hartshorn, M. A., Tyndall, J. D., Hanson, G. R., Stokes, K. C., Leopold, M., Multhaup, G., Goldstein, L. E., Scarpa, R. C., Saunders, A. J., Lim, J., Moir, R. D., Glabe, C., Bowden, E. F., Masters, C. L., Fairlie, D. P., Tanzi, R. E., and Bush, A. I. (1999) *J. Biol. Chem.* **274,** 37111–37116
13. Meloni, G., Sonois, V., Delaine, T., Guilloreau, L., Gillet, A., Teissié, J., Faller, P., and Vasák, M. (2008) *Nat. Chem. Biol.* **4,** 366–372
14. Opazo, C., Huang, X., Cherny, R. A., Moir, R. D., Roher, A. E., White, A. R., Cappai, R., Masters, C. L., Tanzi, R. E., Inestrosa, N. C., and Bush, A. I. (2002) *J. Biol. Chem.* **277,** 40302–40308
15. Smith, D. P., Ciccotosto, G. D., Tew, D. J., Fodero-Tavoletti, M. T., Johanssen, T., Masters, C. L., Barnham, K. J., and Cappai, R. (2007) *Biochemistry* **46,** 2881–2891
16. Smith, D. P., Smith, D. G., Curtain, C. C., Boas, J. F., Pilbrow, J. R., Ciccotosto, G. D., Lau, T. L., Tew, D. J., Perez, K., Wade, J. D., Bush, A. I., Drew, S. C., Separovic, F., Masters, C. L., Cappai, R., and Barnham, K. J. (2006) *J. Biol. Chem.* **281,** 15145–15154
17. Yoshiike, Y., Tanemura, K., Murayama, O., Akagi, T., Murayama, M., Sato, S., Sun, X., Tanaka, N., and Takashima, A. (2001) *J. Biol. Chem.* **276,** 32293–32299
18. Shankar, G. M., Li, S., Mehta, T. H., Garcia-Munoz, A., Shepardson, N. E., Smith, I., Brett, F. M., Farrell, M. A., Rowan, M. J., Lemere, C. A., Regan, C. M., Walsh, D. M., Sabatini, B. L., and Selkoe, D. J. (2008) *Nat. Med.* **14,** 837–842
19. Schlief, M. L., Craig, A. M., and Gitlin, J. D. (2005) *J. Neurosci.* **25,** 239–246
20. Schlief, M. L., West, T., Craig, A. M., Holtzman, D. M., and Gitlin, J. D. (2006) *Proc. Natl. Acad. Sci. U.S.A.* **103,** 14919–14924
21. Crouch, P. J., Hung, L. W., Adlard, P. A., Cortes, M., Lal, V., Filiz, G., Perez, K. A., Nurjono, M., Caragounis, A., Du, T., Laughton, K., Volitakis, I., Bush, A. I., Li, Q. X., Masters, C. L., Cappai, R., Cherny, R. A., Donnelly, P. S., White, A. R., and Barnham, K. J. (2009) *Proc. Natl. Acad. Sci. U.S.A.* **106,** 381–386
22. Pimplikar, S. W. (2009) *Int. J. Biochem. Cell Biol.* **41,** 1261–1268
23. Lim, K. H., Kim, Y. K., and Chang, Y. T. (2007) *Biochemistry* **46,** 13523–13532
24. Sarell, C. J., Wilkinson, S. R., and Viles, J. H. (2010) *J. Biol. Chem.* **285,** 41533–41540
25. Ha, C., Ryu, J., and Park, C. B. (2007) *Biochemistry* **46,** 6118–6125
26. Zou, J., Kajita, K., and Sugimoto, N. (2001) *Angew. Chem. Int. Ed.* **40,** 2274–2277
27. Pedersen, J. T., Teilum, K., Heegaard, N. H. H., Østergaard, J., Adolph, H. W., and Hemmingsen, L. (2011) *Angew. Chem. Int. Ed.* **50,** 2532–2535
28. Matsumura, S., Shinoda, K., Yamada, M., Yokojima, S., Inoue, M., Ohnishi, T., Shimada, T., Kikuchi, K., Masui, D., Hashimoto, S., Sato, M., Ito, A., Akioka, M., Takagi, S., Nakamura, Y., Nemoto, K., Hasegawa, Y., Takamoto, H., Inoue, H., Nakamura, S., Nabeshima, Y., Teplow, D. B., Kinjo, M., and Hoshi, M. (2011) *J. Biol. Chem.* **286,** 11555–11562
29. Necula, M., Kayed, R., Milton, S., and Glabe, C. G. (2007) *J. Biol. Chem.* **282,** 10311–10324
30. Sandberg, A., Luheshi, L. M., Söllvander, S., Pereira de Barros, T., Macao, B., Knowles, T. P., Biverstål, H., Lendel, C., Ekholm-Petterson, F., Dubnovitsky, A., Lannfelt, L., Dobson, C. M., and Härd, T. (2010) *Proc. Natl. Acad. Sci. U.S.A.* **107,** 15595–15600
31. Faller, P. (2009) *ChemBioChem* **10,** 2837–2845
32. Karr, J. W., Kaupp, L. J., and Szalai, V. A. (2004) *J. Am. Chem. Soc.* **126,** 13534–13538
33. Atwood, C. S., Scarpa, R. C., Huang, X., Moir, R. D., Jones, W. D., Fairlie, D. P., Tanzi, R. E., and Bush, A. I. (2000) *J. Neurochem.* **75,** 1219–1233
34. Hatcher, L. Q., Hong, L., Bush, W. D., Carducci, T., and Simon, J. D. (2008)

J. Phys. Chem. B **112,** 8160–8164

35. Huang, X., Atwood, C. S., Hartshorn, M. A., Multhaup, G., Goldstein, L. E., Scarpa, R. C., Cuajungco, M. P., Gray, D. N., Lim, J., Moir, R. D., Tanzi, R. E., and Bush, A. I. (1999) *Biochemistry* **38,** 7609–7616

36. Hurvich, C. M., and Tsai, C. L. (1989) *Biometrika* **76,** 297–307

37. Johnson, K. A., Simpson, Z. B., and Blom, T. (2009) *Anal. Biochem.* **387,** 20–29

38. Morris, A. M., Watzky, M. A., Agar, J. N., and Finke, R. G. (2008) *Biochemistry* **47,** 2413–2427

39. Karr, J. W., and Szalai, V. A. (2008) *Biochemistry* **47,** 5006–5016

40. LeVine, H., 3rd (2004) *Anal. Biochem.* **335,** 81–90

41. Seubert, P., Vigo-Pelfrey, C., Esch, F., Lee, M., Dovey, H., Davis, D., Sinha, S., Schlossmacher, M., Whaley, J., Swindlehurst, C., *et al.* (1992) *Nature* **359,** 325–327

42. Miura, T., Suzuki, K., Kohata, N., and Takeuchi, H. (2000) *Biochemistry* **39,** 7024–7031

43. Chen, W. T., Liao, Y. H., Yu, H. M., Cheng, I. H., and Chen, Y. R. (2011) *J. Biol. Chem.* **286,** 9646–9656

44. Talmard, C., Guilloreau, L., Coppel, Y., Mazarguil, H., and Faller, P. (2007) *ChemBioChem* **8,** 163–165

45. Biancalana, M., Makabe, K., Koide, A., and Koide, S. (2009) *J. Mol. Biol.* **385,** 1052–1063

46. Brzyska, M., Trzesniewska, K., Wieckowska, A., Szczepankiewicz, A., and Elbaum, D. (2009) *ChemBioChem* **10,** 1045–1055

47. Bitan, G., Kirkitadze, M. D., Lomakin, A., Vollers, S. S., Benedek, G. B., and Teplow, D. B. (2003) *Proc. Natl. Acad. Sci. U.S.A.* **100,** 330–335

48. Chimon, S., Shaibat, M. A., Jones, C. R., Calero, D. C., Aizezi, B., and Ishii, Y. (2007) *Nat. Struct. Mol. Biol.* **14,** 1157–1164

49. Raman, B., Ban, T., Yamaguchi, K., Sakai, M., Kawai, T., Naiki, H., and Goto, Y. (2005) *J. Biol. Chem.* **280,** 16157–16162

50. Jun, S. M., and Saxena, S. (2007) *Angew. Chem. Int. Ed.* **46,** 3959–3961

51. Groenning, M. (2010) *J. Chem. Biol.* **3,** 1–18

52. Karr, J. W., Akintoye, H., Kaupp, L. J., and Szalai, V. A. (2005) *Biochemistry* **44,** 5478–5487

53. Kowalik-Jankowska, T., Ruta, M., Wiśniewska, K., and Lankiewicz, L. (2003) *J. Inorg. Biochem.* **95,** 270–282

54. Syme, C. D., Nadal, R. C., Rigby, S. E., and Viles, J. H. (2004) *J. Biol. Chem.* **279,** 18169–18177

55. Guilloreau, L., Damian, L., Coppel, Y., Mazarguil, H., Winterhalter, M., and Faller, P. (2006) *J. Biol. Inorg. Chem.* **11,** 1024–1038

56. Kirschner, D. A., Inouye, H., Duffy, L. K., Sinclair, A., Lind, M., and Selkoe, D. J. (1987) *Proc. Natl. Acad. Sci. U.S.A.* **84,** 6953–6957

57. Shen, C. L., Scott, G. L., Merchant, F., and Murphy, R. M. (1993) *Biophys. J.* **65,** 2383–2395

58. Faller, P., and Hureau, C. (2009) *Dalton Trans.* **7,** 1080–1094

59. Balbach, J. J., Ishii, Y., Antzutkin, O. N., Leapman, R. D., Rizzo, N. W., Dyda, F., Reed, J., and Tycko, R. (2000) *Biochemistry* **39,** 13748–13759

60. Ostergaard, J., and Heegaard, N. H. (2006) *Electrophoresis* **27,** 2590–2608

61. Tõugu, V., Karafin, A., Zovo, K., Chung, R. S., Howells, C., West, A. K., and Palumaa, P. (2009) *J. Neurochem.* **110,** 1784–1795

62. Drew, S. C., Noble, C. J., Masters, C. L., Hanson, G. R., and Barnham, K. J. (2009) *J. Am. Chem. Soc.* **131,** 1195–1207

63. Karr, J. W., and Szalai, V. A. (2007) *J. Am. Chem. Soc.* **129,** 3796–3797

64. Dorlet, P., Gambarelli, S., Faller, P., and Hureau, C. (2009) *Angew. Chem. Int. Ed.* **48,** 9273–9276

65. Dong, J., Canfield, J. M., Mehta, A. K., Shokes, J. E., Tian, B., Childers, W. S., Simmons, J. A., Mao, Z., Scott, R. A., Warncke, K., and Lynn, D. G. (2007) *Proc. Natl. Acad. Sci. U.S.A.* **104,** 13313–13318

66. Capanni, C., Taddei, N., Gabrielli, S., Messori, L., Orioli, P., Chiti, F., Stefani, M., and Ramponi, G. (2004) *Cell. Mol. Life Sci.* **61,** 982–991

67. Frieden, C. (1985) *Annu. Rev. Biophys. Biophys. Chem.* **14,** 189–210

68. D'Andrea, M. R., Nagele, R. G., Wang, H. Y., Peterson, P. A., and Lee, D. H. (2001) *Histopathology* **38,** 120–134

69. Walsh, D. M., Tseng, B. P., Rydel, R. E., Podlisny, M. B., and Selkoe, D. J. (2000) *Biochemistry* **39,** 10831–10839

70. LaFerla, F. M., Green, K. N., and Oddo, S. (2007) *Nat. Rev. Neurosci.* **8,** 499–509

71. Eakin, C. M., Knight, J. D., Morgan, C. J., Gelfand, M. A., and Miranker, A. D. (2002) *Biochemistry* **41,** 10646–10656

72. Viles, J. H., Klewpatinond, M., and Nadal, R. C. (2008) *Biochem. Soc. Trans.* **36,** 1288–1292

73. Paik, S. R., Shin, H. J., Lee, J. H., Chang, C. S., and Kim, J. (1999) *Biochem. J.* **340,** 821–828